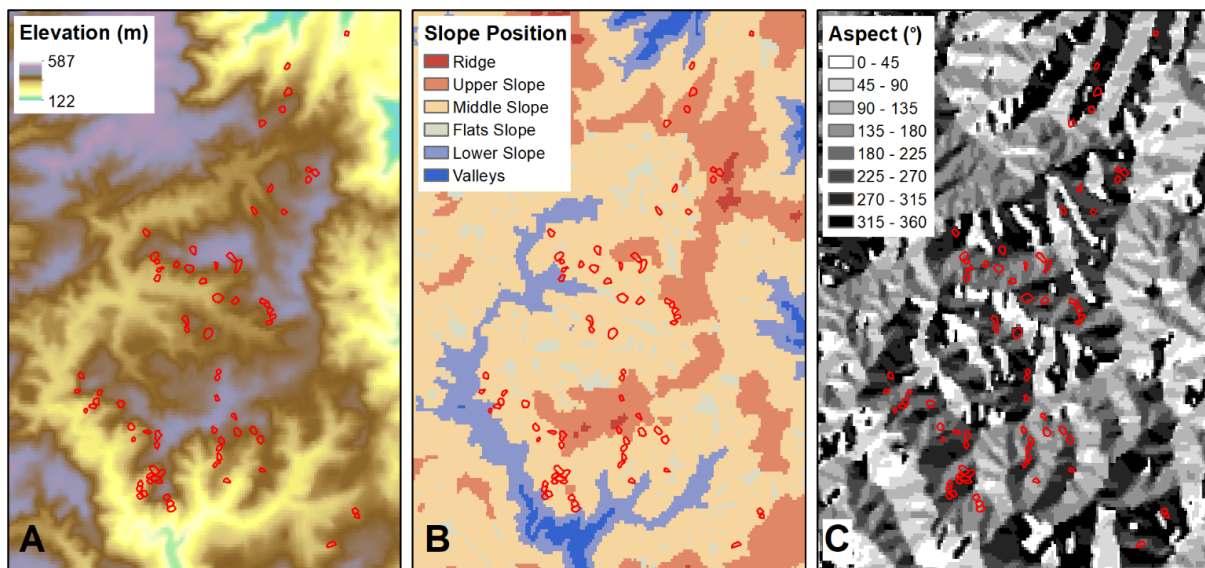


Red Needle Cast monitoring framework using high resolution satellite imagery

Ellen Mae Leonardo, Grant Pearse, Stuart Fraser and Honey Jane Estarija



Date: 19 June 2020

Report No: RFP-T008

TABLE OF CONTENTS

EXECUTIVE SUMMARY	1
INTRODUCTION	2
Objective.....	2
Data	3
Method.....	5
RESULTS	7
DISCUSSION	13
Next Steps	14
ACKNOWLEDGEMENTS	15

Disclaimer

This report has been prepared by New Zealand Forest Research Institute Limited (Scion) for Forest Growers Research Ltd (FGR) subject to the terms and conditions of a research fund agreement dated 1 April 2014.

The opinions and information provided in this report have been provided in good faith and on the basis that every endeavour has been made to be accurate and not misleading and to exercise reasonable care, skill and judgement in providing such opinions and information.

Under the terms of the Services Agreement, Scion's liability to FGR in relation to the services provided to produce this report is limited to the value of those services. Neither Scion nor any of its employees, contractors, agents or other persons acting on its behalf or under its control accept any responsibility to any person or organisation in respect of any information or opinion provided in this report in excess of that amount.



EXECUTIVE SUMMARY

A framework for the use of high-resolution satellite imagery for the detection and monitoring of red needle cast (RNC) is presented. The methodology was tested for three sites on the east coast of the North Island, namely, Waimata Valley Road, Wharerata, and Tauwhareparae, where ground observations were made in September 2018 and 2019. Using training samples selected for each imagery, a set of threshold-based classification rules for the different surface reflectance bands and vegetation indices were identified for each site. Object-based classification was then used to segment the whole images into objects or groups of pixels with the same characteristics and the threshold rules were applied to separate different classes and identify unhealthy patches of radiata pine trees that are suspected to be affected by RNC. The accuracy of unhealthy tree detection within the three sites varied from 60.0 to 93.0% and the false positive rate was estimated to be between 6.7 to 9.5%. This work demonstrated the possibility of using single-scene satellite images to identify possible forest areas affected by the disease.

The initial results presented in this paper also highlighted the importance of having repeated image acquisition and field measurements to generate a more robust classifier. Comparing the recurring samples of infected tree patches with the elevation data and derived terrain metrics can help identify at-risk surfaces and establish information that can be useful in disease prediction models.

The proposed next steps are to continue the disease observations to identify the severity and peak expression then acquire new imagery to produce new classification maps that will guide targeted ground truthing. This simple and repeatable method expands the range of annual RNC monitoring which is a key requirement for improving predictive models and assessing the landscape-level impacts of disease.

INTRODUCTION

Red needle cast (RNC), caused by *Phytophthora pluvialis*, has emerged as a serious foliar pathogen of radiata pine in New Zealand (Dick, et al., 2014). Previous work at Scion involved utilising data from forest health monitoring sites to understand drivers of the pathogen and build predictive models to inform management activities. Development of these models highlighted the need for a greater number of observations of the disease covering a wider range of environmental gradients. Existing data lacked spatially explicit information and were often limited to localised detections from roadside observation points. The observed symptoms of RNC are variable and can range from isolated trees with little needle loss to large stands with extensive defoliation. Remote sensing offers a relatively cost-effective means of overcoming these issues by monitoring larger areas using imagery with the intended scale of the surveillance determining the required resolution.

Scion has integrated remote sensing-based monitoring techniques at a range of scales. Existing trials studying copper control of RNC are routinely assessed using very high resolution (< 5cm) multispectral imagery from manned or unmanned aircraft to score severity at the tree level and these methods will be extended to the planned sensor network trial outlined in Resilient Forests RA3 (Sellier, et al., 2020). Larger scale studies have also demonstrated the utility of open data from the European Space Agency's Sentinel-2 platform for detecting outbreaks, but this work highlighted the need for higher-resolution data to detect more localised outbreaks across the landscape.

Objective

This Technical Report outlines recent work at Scion utilising high-resolution satellite imagery to detect and map moderate to large-scale outbreaks of RNC as a means of increasing surveillance efforts and expanding the geographic and environmental gradients covered in the database. With the expansion of high-resolution satellite imagery data sources, it is increasingly cost-effective to utilise satellite-based observation for forest health monitoring. The resolution of this imagery allows detection to be carried out at finer scales ranging from single trees to small patches. This can be achieved using two general approaches. Firstly, algorithms such as BFAST (Verbesselt, et al., 2010) or LandTrendr (Kennedy, et al., 2010) can be used with time-series imagery to detect anomalies such as disease outbreaks within broader trends. These methods are most useful with data sources such as Landsat or Sentinel-2 that offer free access to long-term datasets. This approach will be used for landscape and regional-level monitoring in RA3.2. An alternative approach, outlined in this technical note, uses a single scene imagery combined with training data to identify areas of forest affected by disease. This method has the advantage of only requiring a single image to be purchased and is not affected by issues such as missing or low-quality imagery in the temporal image series. The objective of this work was to develop a repeatable and efficient process for ingesting imagery acquired at multiple locations across New Zealand and producing maps of areas with moderate to severe RNC severity. The intention is to target ground sampling to these identified areas to confirm the observations and positively identify the causal pathogen(s). These data will then be used for purposes such as expanding the data available to develop risk surfaces and predictive models for RNC and to study the longer-term impacts of RNC on forest productivity. By repeating this analysis at the sensor network sites, we will be able to establish important links between the spectral changes observed (e.g. changes in vegetation indices) with changes in foliage dynamics and tree growth measured at these locations. This is important to calibrate the sensitivity of imagery-based detection in terms of scale and severity and evaluate the potential for scaling impact assessments to the landscape level.

Data

Study areas

Three study sites near the east coast of the North Island, New Zealand were identified as the areas of interest (AOIs) for selection of available archived satellite imagery to acquire. These were Tauwhareparae, Waimata Valley Road, and Wharerata (Fig. 1).

Field records

Road-side field observations of RNC severity within the AOIs were recorded in October in 2015, and September in 2016, 2017, 2018, and 2019. The data consisted of site name, location in terms of Easting and Northing, estimated age, date, and disease index.

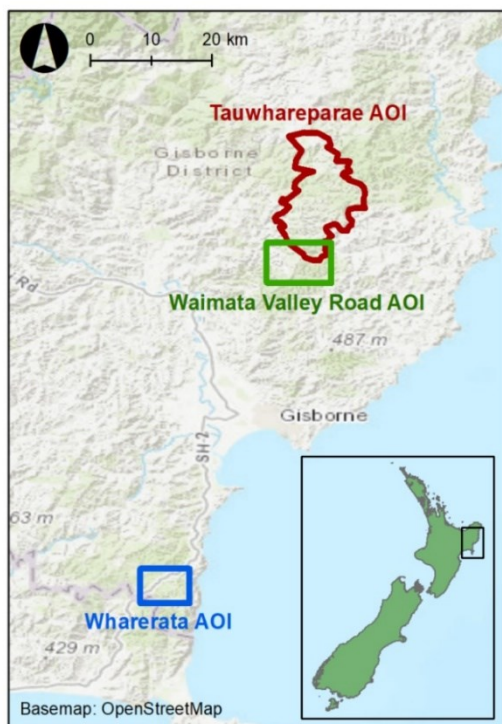


Fig. 1. Location of the three AOIs: Tauwhareparae (red outline), Waimata Valley Road (green), and Wharerata (blue).

Satellite images

The field observations were used to identify years with moderate to severe disease expression and select satellite images for developing and testing RNC observation and detection methods. Therefore, the image searches in the AOIs were limited to 2015 to 2019 in the months of September to December when RNC symptoms were most evident. Filters relating to the usability and quality of the satellite images were also applied in the search. The first filter was the off-nadir angle which determines if the satellite is looking down to the target directly (nadir, 0°) or at angle. High off-nadir angles exaggerate shadows in the images due to the terrain variability. The off-nadir filter applied included only images with off-nadir angle $< 30^\circ$. The second filter was the sun elevation or the angle above the horizon. Sun elevation angles that are too low can cause the images to be too dark, therefore the filter was set to include images with elevation $> 30^\circ$. Cloud filter ($< 10\%$) and AOI coverage filters ($> 90\%$) were also applied. The archived imagery that met these criteria were visually inspected using previews to assess the quality and evidence of visible RNC symptoms. Two images for Tauwhareparae, one image for Waimata Valley Road, and two images for Wharerata were determined to be suitable for RNC detection and were purchased for analysis (Table 1).

Table 1. Satellite images acquired with their corresponding AOI and dates

Location	Satellite	Date
Tauwhareparae	Worldview-3	12-09-2019
Tauwhareparae	Geoeye-1	04-12-2018
Waimata Valley Road	Worldview-3	12-09-2019
Wharerata	Worldview-2	15-09-2019
Wharerata	Worldview-2	13-09-2018

The selected images are products from three different satellites: Worldview-3 (WV-3), Worldview-2 (WV-2), and GeoEye-1 (GEO). The Worldview products have eight spectral bands while GEO only has four. The spectral bands with their specific wavelengths are shown in Table 2. All the products have panchromatic bands which is a wide-range band with a higher spatial resolution of 50 cm that can be used to pansharpen the other bands to increase their 2 m native spatial resolution to 50 cm.

Table 2. Spectral bands and corresponding wavelengths of the Worldview and GeoEye products

Worldview-2 & 3	
Spectral Bands	Wavelength (nm)
Coastal	400 – 450
Blue	450 – 510
Green	510 – 580
Yellow	585 – 625
Red	630 – 690
Red Edge	705 – 745
NIR 1	770 – 895
NIR 2	860 – 1040
Panchromatic	450 – 800
GeoEye-1	
Spectral Bands	Wavelength (nm)
Blue	450 – 510
Green	510 – 580
Red	655 – 690
NIR	780 – 920
Panchromatic	450 – 800

Elevation raster data

A Digital Elevation Model (DEM) raster dataset at 25 m spatial resolution of the whole of New Zealand was downloaded from the Land Resource Information Systems (LRIS) Portal (<https://iris.scinfo.org.nz/>).

The data were processed to derive slope, aspect, and topographic position index (TPI).

Method

Processing of satellite datasets

The images provided by the supplier were in the form of atmospherically corrected surface reflectance through their proprietary atmospheric compensation (AComp) algorithm. AComp is a fully automated method that estimates the surface reflectance of a portion of an image and iteratively adjusts the aerosol optical depth (AOD) setting of the image based on this value (Digital Globe, 2016; Pacifici, 2016).

Scion's existing processes have utilised FLAASH atmospheric correction. A comparison of FLAASH applied to unprocessed source imagery and the ACOMP products showed the two methods to be comparable and ACOMP was selected based on the reduced processing requirements.

From the surface reflectance rasters, the vegetation indices were calculated using the NDVI/Spectral Indices toolbox in ENVI 5.5.3. Normalised Difference Vegetation Index (NDVI), Green Normalised Difference Vegetation Index (GNDVI), Red-Edge Normalised Difference Vegetation Index (RENDVI), and Enhanced Vegetation Index (EVI) were calculated using the equations:

$$NDVI = \frac{NIR - Red}{NIR + Red}$$

$$GNDVI = \frac{NIR - Green}{NIR + Green}$$

$$RENDVI = \frac{NIR - Red\ Edge}{NIR + Red\ Edge}$$

$$EVI = Green \times \frac{NIR - Red}{NIR + C_1 \times Red - C_2 \times Blue + L}$$

where NIR is band 7 for WV and band 4 for GEO, Green is band 3 for WV and band 2 for GEO, Red is band 5 for WV and band 1 for GEO, Red Edge is band 6 for WV, and C_1 , C_2 , and L are coefficients for atmospheric resistance and canopy background.

Masking of shadows was done by applying a threshold to the reflectance values of each pixel. The threshold was determined by manually sampling shadow pixels and non-shadow patches from areas containing healthy and infected trees, grassland, bare soil, roads, native trees. Histograms of the reflectance in different bands were produced and thresholds were selected to maximise the separation of shadow and non-shadow pixels. A scene-wide shadow mask was then applied to the reflectance maps and derived vegetation indices to exclude all shadow pixels from further analysis.

For further detailed analysis, the reflectance maps were pansharpened using their corresponding panchromatic bands. This was executed in ENVI 5.5.3 using the Gram-Schmidt Pan Sharpening tool. The process of pansharpening resulted in increased detail in the images but the spectral information was altered making it unsuitable for further spectral analysis.

Creation of labelled samples

Labelled samples for six cover classes were created to serve as input for a land cover classifier. The actual locations of these were identified based on visual interpretation of the pansharpened and native-resolution natural-colour image in ArcGIS Pro 2.5.1, as well as other ancillary sources of imagery.

The classes were designated as *healthy pine trees*, *unhealthy pine trees* which were assumed to be infected by the disease, *other trees* which include native vegetation and other woody weeds, *grass*, *roads*, and *bare soil*. Groups of pixels that represented patches of unhealthy pine trees were first identified. The total number of samples for this class is based on the land area of each site and the severity of the disease infection observed by inspecting the whole satellite image. After this, the same number of samples for each of the other classes were added. The total numbers of labelled samples were 770 for Waimata, 560 for Wharerata, and 910 for Tauwhareparae. For each site, a subset of 30 labelled samples per class were randomly set aside from the training data as a validation dataset to assess the accuracy of the classifier.

Classification of red needle cast

The approach to identify the unhealthy trees from other classes were divided into two parts. The first part consists of shadow masking the rasters and using zonal statistics to identify the statistical distribution of reflectance values for each sample feature. This was implemented using the `arcpy` module in Python 2.7 and the results were used to determine the classification rules. The second part utilised object-based analysis to split the images into similar areas or objects (e.g. pixels within a canopy), before applying a rule-based classification at the object level rather than the pixel level. This improves the consistency and coherence of classification and avoids single misclassified pixels surrounded by a majority class. The reflectance rasters, panchromatic band, and vegetation indices were all included as input data for the object-based classifier. Segmentation was first executed based on the Red, Green, Blue, and near-infrared (NIR) bands, panchromatic band, and vegetation indices. The rule-based classification was then implemented to (1) differentiate non-vegetation from vegetation objects, (2) differentiate grass from trees, (3) differentiate native trees from planted radiata, and finally (4) differentiate healthy and unhealthy radiata pine trees. The rules were based on thresholds that were identified from the statistical distribution of the values per band that fell within the sample objects. They are, therefore, image/site-dependent. The segmentation and classification were implemented in eCognition Developer 9.3.

Derivation of elevation and terrain metrics

From the 25 m DEM datasets, slope and aspect rasters were derived using the GDAL DEM library for raster and vector geospatial data (<https://gdal.org/>). The default parameters for slope and aspect calculations were applied. The DEM and slope rasters were then used to compute the topographic position index (TPI) and its classification. TPI was calculated using the SAGA-GIS library in terrain analysis and morphometry (<http://www.saga-gis.org/>). TPI is a metric that classifies location within the landscape while allowing for the scale-dependent nature of this exercise. For example, at a large scale a site may be flat but at smaller scales (e.g. landscape) it may be positioned mid-slope. Position in the terrain has previously been highlighted as a potential proxy for RNC severity. Our working hypothesis was that terrain positions that favour formation and flow of moist air across the canopy surface may increase the transmission and reproduction of RNC. TPI was computed at 1 km scale and each pixel was classified into slope positions, namely, ridge, upper slope, middle slope, flats slope, lower slope, and valleys based on the TPI value compared to the standard deviation across the whole dataset and slope.

RESULTS

Forest and Shadow Masking of Satellite Images

The threshold-based shadow masking approach was applied using the difference between red (R), green (G), blue (B), and near-infrared (NIR) surface reflectance in sunlit and shadow areas (Fig. 2).

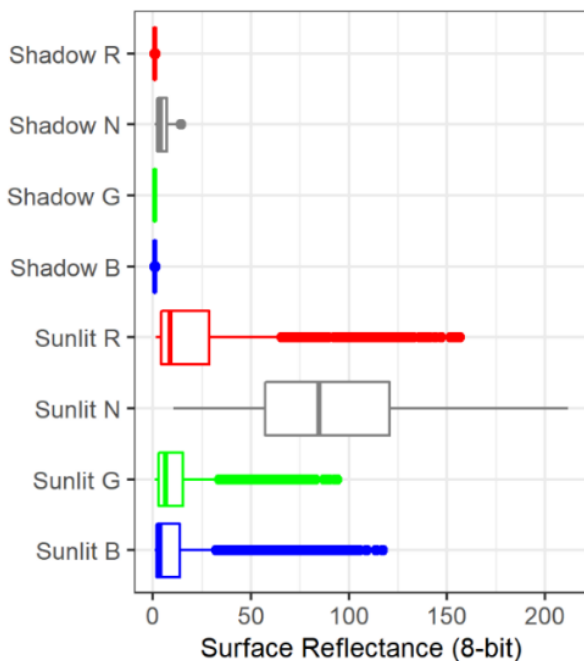


Fig. 2. Boxplot of Red, Green, Blue, and NIR (RGB-NIR) surface reflectance values for the differentiation between shadow and sunlit pixels in the Waimata AOI.

For the remaining sunlit pixels, a vegetation mask was derived using a combination of vegetation indices (e.g. NDVI and EVI for the Waimata AOI). From these vegetation pixels, a radiata forest mask was derived to exclude grass and other trees. This is to avoid misclassification of unhealthy pine trees which also have lower vegetation indices similar to grass and other vegetation. For example, the Waimata AOI classification separated grass from other vegetation pixels using the yellow, green, and panchromatic band. On the other hand, other trees that include natives, invasives, and other woody weeds, were differentiated from radiata pine forest by utilising blue, NIR1, GNDVI, and RENDVI thresholds. Fig. 3 shows the distribution of RENDVI values per vegetative class as one of the indices used to derive the radiata pine forest mask shown in Fig. 4.



Fig. 3. Boxplot of RENDVI for each vegetation class for Waimata AOI

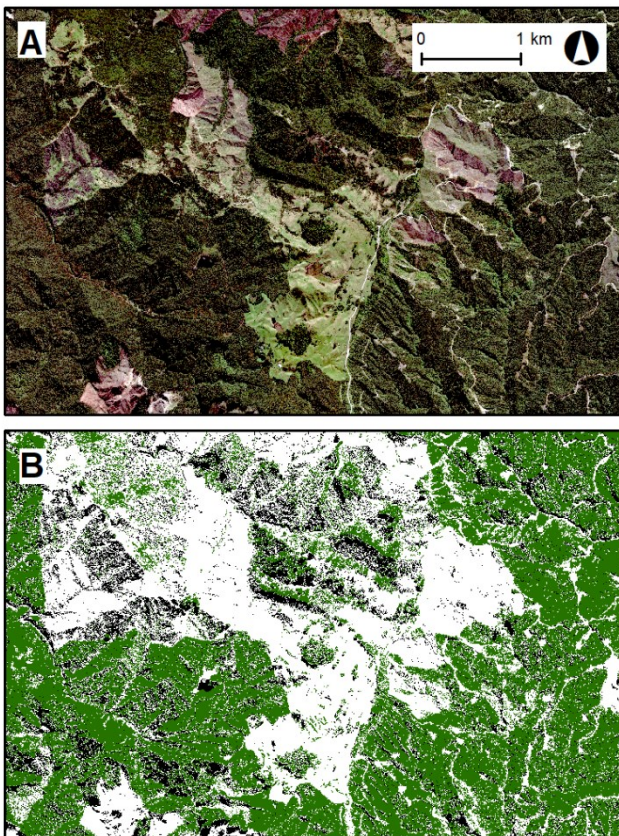


Fig. 4. A portion of Waimata area showing the RGB image (a) and derived forest and shadow mask (b). Areas classified as radiata forest are shown in green with shadows in black in the masked image. Other vegetation areas such as native forests are colour white.

Differentiation between healthy and infected trees

Within the remaining radiata forest pixels, there was a clear delineation between healthy vegetation and unhealthy vegetation patches that are possibly infected by red needle cast when it comes to the vegetation indices, especially NDVI which was used in all sites (Fig. 5). This was the final rule that was implemented to create the classification maps in the next sections.

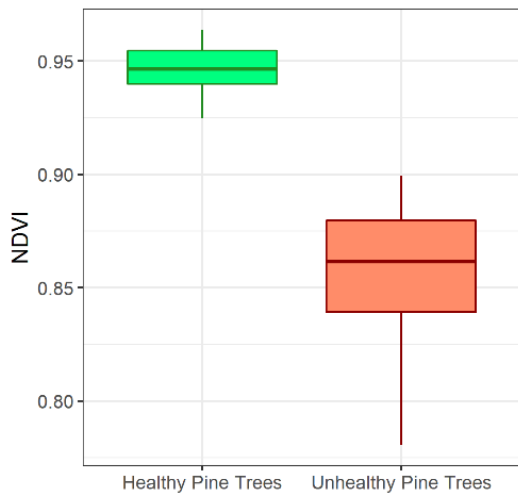


Fig. 5. Boxplot of NDVI for healthy and unhealthy radiata pine trees for Waimata AOI

Classification of RNC in Waimata AOI

The imagery used to detect RNC in Waimata showed large areas of affected trees (Fig. 6). Using the 30 withheld areas labelled as unhealthy for validation, the classifier showed 93.3% accuracy in detecting unhealthy trees (Table 4). Fig. 6 shows a close-up view of a heavily affected area, while Fig. 7 shows the classification in the whole AOI. Applying the classifier to the whole AOI in Fig. 7 highlighted other possible localised areas of disease across the AOI.

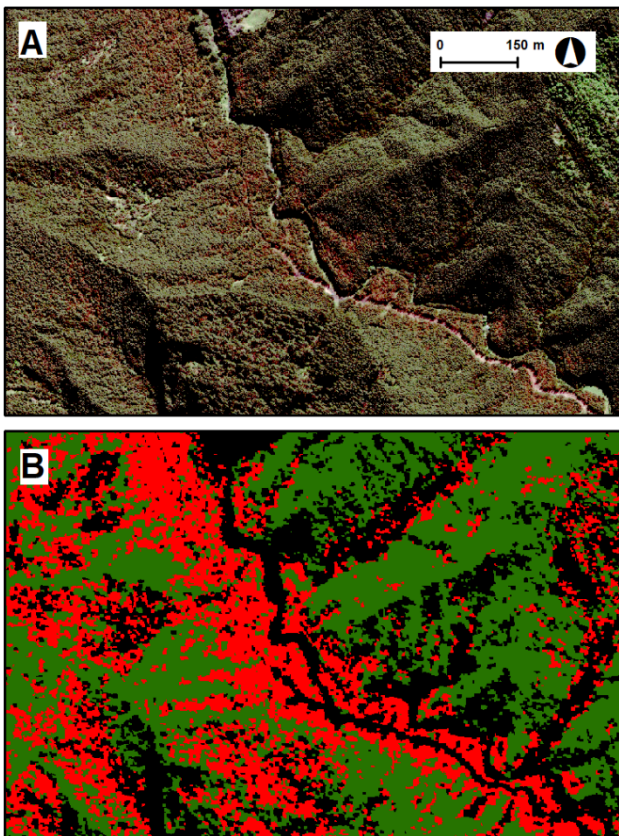


Fig. 6. Close-up view of a heavily RNC infected area in the Waimata AOI. The top image is the pansharpened RGB image while the bottom image shows its corresponding classification map where the green pixels represent the healthy trees while the red pixels represent the affected trees.

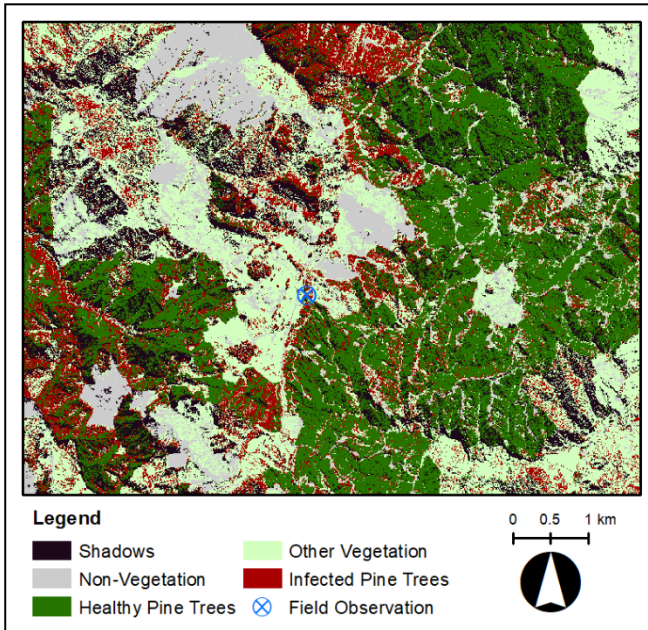


Fig. 7. Classification map in Waimata AOI

Table 4 shows the confusion matrix for the rule-based classification method applied to both the training and validation data. The classifier correctly identified all healthy tree patches and misclassifications into this class were rare. A small percentage of unhealthy tree patches were misclassified while objects from other classes (i.e. bare soil, road, native trees, and grass) were more often misclassified as unhealthy trees. This suggests that there is a moderate probability of false detection of RNC affected areas, strengthening the need for field validation in monitored areas.

Table 4. Accuracy assessment for classification in Waimata AOI

Training Data

		Reference			
		Healthy	Unhealthy	Others	Total
Predicted	Healthy	80	2	2	84
	Unhealthy	0	75	18	93
	Others	0	3	300	303
	Total	80	80	320	480
	Accuracy	100%	93.8%	93.8%	-

Validation Data

		Reference			
		Healthy	Unhealthy	Others	Total
Predicted	Healthy	30	2	2	34
	Unhealthy	0	28	6	34
	Others	0	0	112	112
	Total	30	30	120	180
	Accuracy	100%	93.3%	93.3%	-

Classification of RNC in Wharerata

GNDVI and NDVI were used as thresholds in differentiating healthy and unhealthy pine trees in Wharerata for both 2018 and 2019 maps (Fig. 8). For the 2018 classification, the disease detection was less accurate than Waimata (73.3%) and 8.3% of the total infected predictions were false positives. Therefore, the disease classification in Fig 8a might be overestimated in some areas. The healthy trees, similar to the Waimata classification, were all predicted accurately.

The same set of rules were applied in the classification of the Wharerata image in 2019 (Fig. 8b). There were no feature annotations in this image as minimal RNC symptoms were visually identified. The output map shows some extent of affected areas, but these are most likely misclassified grass or trees that are not radiata pine. The overall difference of the 2018 and 2019 classification supports the field observation where the disease index assigned to 2018 were 14 & 85.5 and were reduced to 0.75 and 60 in 2019.

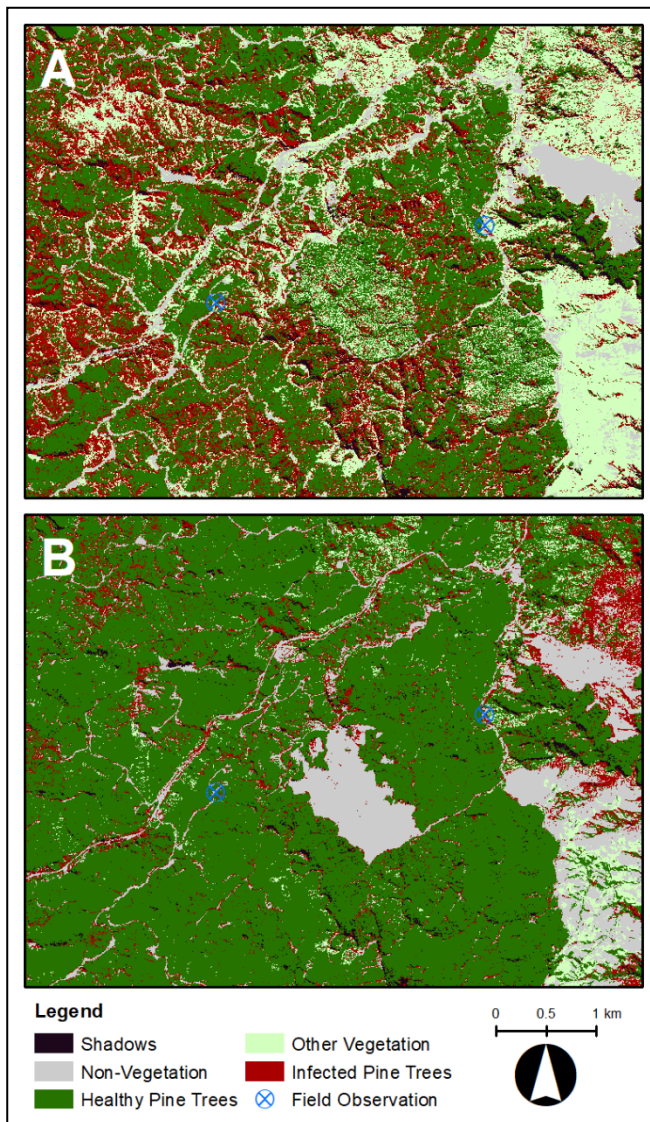


Fig. 8. Classification map in Wharerata AOI in 2018 (a) and in 2019 (b)

Classification of RNC in Tauwhareparae

Similar to the Wharerata classification, GNDVI and NDVI were the key vegetation indices used to differentiate unhealthy forest patches from healthy ones in the Tauwhareparae AOI. The classifier in this location had a 9.5% rate of false positives and a lower sensitivity to RNC (60%). The Tauwhareparae classification map in Fig. 9 shows that there are minimal pixels that represent the affected tree patches in the northeast part of the AOI where the roadside assessments were undertaken. Furthermore, another area of possible RNC infection that is more severe can be located in the southwest part of the AOI (Fig 9).

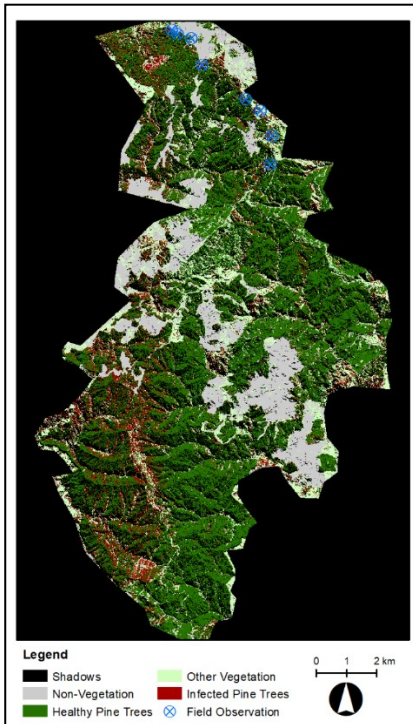


Fig. 9. Classification map in Tauwhareparae AOI in 2019

Terrain Analysis

The distribution of unhealthy tree patches was examined in the Wharerata AOI. The labelled sample patches were used instead of the classification results to avoid including the false positives and false negatives. Some patterns emerged as shown in Fig. 10. For example, many of the sample patches of unhealthy trees were located on mid-slope areas with the slope values are higher than 10° . The unhealthy patches also appeared to be located in areas where the aspect ranges from 135 to 270° or areas that are facing southeast to west. The results from the analysis were added to a database that will be used to provide additional observations for the modelling framework developed in RA3.

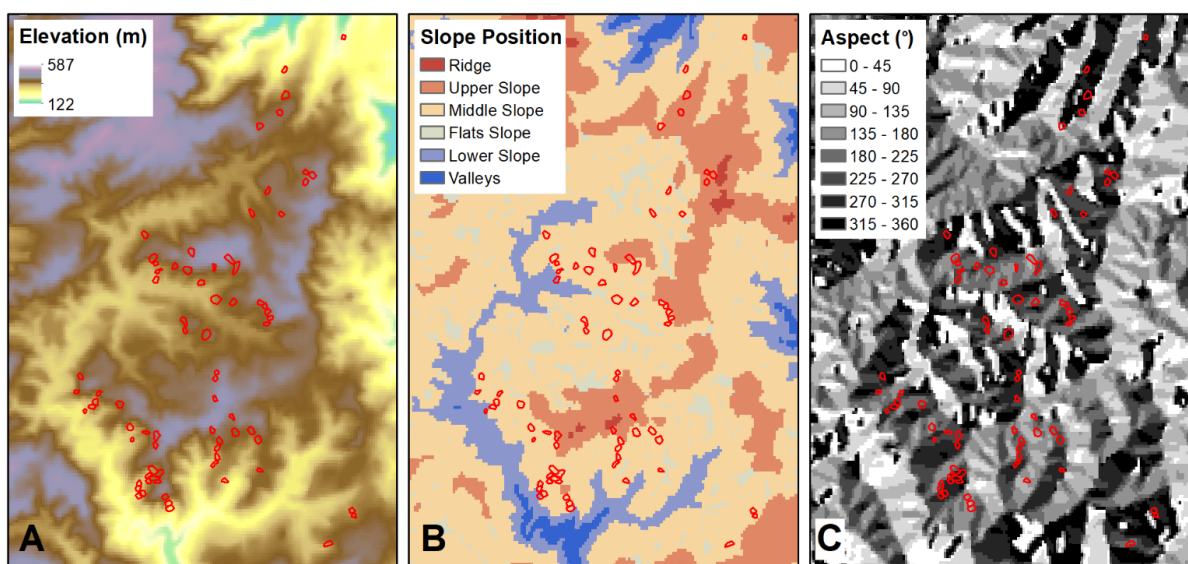


Fig. 10. Sample annotations of affected tree patches (red outlines) overlaid on elevation raster (left), slope position calculated from TPI (middle), and aspect (right) in Wharerata AOI.

DISCUSSION

A method for object-based classification created from decision rules for classifying satellite imagery and detecting local areas of RNC expression was developed and applied to three study sites where ground assessments were undertaken in September 2018 and 2019. This work demonstrated the possibility of using single-scene satellite images and training data to identify forest areas that are affected by disease.

The accuracy of the classification method in detecting unhealthy forest in all the sites varied from moderate to high (60.0 to 93.3%) with a reasonable false-positive rate (6.7 to 9.5%). This is a good indication of usability of the satellite image classification in identifying local extents of infection. The classification algorithm is currently semi-automated, but it is repeatable and can be further improved through replication and addition of verified field data. Some aspects of the current results, such as the rule-based shadow mask and forest masks (example shown in Fig. 4), were generalised well across sites and can be carried over when new imagery is acquired each year. This is useful in future analysis because only the sunlit forest pixels are needed to detect disease expression. Instead of manually selecting samples of other classes (e.g. bare soil, roads, grass, and trees), the feature selection can be focused on healthy and unhealthy tree patches with different severity. Moreover, the current thresholds for differentiating healthy and unhealthy forest tree patches depend on the image statistics from each spectral band. This makes the thresholding dependent on the image or site. The resulting Wharerata RNC maps did show that the thresholds can be applied to a more recent dataset and still produce a reasonable classification (Fig. 8b). This is one advantage of using atmospherically corrected products where the reflectance values within the same locations are expected to be consistent to some extent over time. Acquiring samples of unhealthy patches with varying degree of severity will allow a more robust threshold to be applied to images in the same location captured during different years.

With repeated image acquisition and measurements, these thresholds can be generalised to be more precise and robust for each site. In effect, the effort and time in feature selection can be significantly reduced until the method can be efficiently automated eventually. The current method is also an exploratory process that is well suited to a low number of training samples. As more data are available, the process will be improved by using more sophisticated machine learning algorithms such as random forest classifier, neural networks, and support vector machines to generate robust classifiers.

Next Steps

An essential part of this methodological framework is the need for validation of the probable areas infected with RNC. The current ground-truth data rely on roadside observations of disease severity. For the 2020 disease season, this approach will be operationalised as part of Scion's monitoring programme. Disease observations from roadside surveillance will be used to identify the severity and peak expression within up to five locations. Imagery will then be acquired and processed to identify RNC using the method outlined. These observations will then be followed up with targeted ground truthing to verify the severity and causal pathogen through laboratory analysis of samples. The maps can guide the field teams in which areas to prioritise over large AOIs such as Tauwhareparae (Fig. 9) and as the classification improves over time and false-positives are minimised, the time and effort in the field validation can also be significantly reduced.

Different remote sensing data sources are available for continued work in local studies of RNC. For instance, the acquisition of satellite imagery can be done frequently and can be targeted with satellite tasking. The rise of new satellite constellations through 2020-2021 by different providers will also mean greatly increased availability of high-resolution datasets. These new data sources can be utilised to enhance regular monitoring of the presence and severity of disease impacts in targeted locations. The utility of satellite images with limited bands (RGB-NIR only, such as GEO) as input for classifiers can also be assessed. If classifications based on limited bands are proved to be in an acceptable level of accuracy, this will further increase the availability of satellite data sources. Additionally, Light Detection and Ranging (LiDAR) measurements of elevation and height are in progress for most areas in New Zealand, particularly in the East Coast. The addition of dense height measurements will be of added benefit for delineating planted radiata forests from other land use classes that will further reduce the false-positive rate.

Linking the elevation data and derived terrain metrics, such as slope, aspect, and TPI along with recurring samples of disease expression can aid in identifying at-risk surfaces and establishing information that can be useful in predictive models. The example shown in Fig. 10, though an oversimplification in a local area in one site, gives an overview to the possible utilisation of this approach for long-term monitoring.

In summary, a feedback process for RNC detection and mapping is proposed with the following steps: (1) ground truthing during the RNC peak season, (2) regular satellite image acquisition of the monitoring sites (e.g. annual), (3) extraction of sunlit forest pixels, (4) sampling of healthy and infected forest patches with different severity, (5) classification to produce the probability map, (6) coordinated field validation of the probability map if needed, and (7) correction in the RNC classification.

This 'virtual' study on RNC detection using high-resolution satellite imagery demonstrates a method to greatly expand the range of annual RNC monitoring using a relatively simple and repeatable approach. This will allow us to expand the method to up to five sites to cover a wider range of sites across New Zealand. This is a key requirement for improving predictive models and assessing the landscape-level impacts.

Outside of this work, a further study using freely available medium resolution time-series imagery will explore the potential to expand satellite-based monitoring to regional scales while utilising techniques relying on time series analysis to detect RNC. This work is under way in resilient forests RA 3.2.

ACKNOWLEDGEMENTS

Funding for this research came from Scion and the Forest Growers Levy Trust, with the support of the NZ Forest Owners Association (FOA) and the NZ Farm Forestry Association (FFA).

References

- Dick, M. A., Williams, N. M., Bader, M. K.-F., Gardner, J. F., & Bulman, L. S. (2014). Pathogenicity of *Phytophthora pluvialis* to *Pinus radiata* and its relation with red needle cast disease in New Zealand. *New Zealand Journal of Forestry Science*, 44(1), 6. doi:10.1186/s40490-014-0006-7
- Digital Globe. *Digital Globe Atmospheric Compensation*. Retrieved May 21, 2020, from http://digitalglobe-marketing.s3.amazonaws.com/files/documents/AComp_WP_ACOMP.pdf
- Kennedy, R. E., Yang, Z., & Cohen, W. B. (2010). Detecting trends in forest disturbance and recovery using yearly Landsat time series: 1. LandTrendr — Temporal segmentation algorithms. *Remote Sensing of Environment*, 114(12), 2897-2910. doi:<https://doi.org/10.1016/j.rse.2010.07.008>
- Pacifici, F. (2016). Atmospheric compensation in satellite imagery: Google Patents.
- Sellier, D., Williams, N., Fraser, S., Hartley, R., Pearse, G., Wright, L., Cotterill, V., Tan, A., Somchit, C., & Graham, N. (2020). *Monitoring the seasonal growth impact of foliar pathogens -- an ideal sensor network*. Unpublished. Technote: Scion.
- Verbesselt, J., Hyndman, R., Zeileis, A., & Culvenor, D. (2010). Phenological change detection while accounting for abrupt and gradual trends in satellite image time series. *Remote Sensing of Environment*, 114(12), 2970-2980. doi:<https://doi.org/10.1016/j.rse.2010.08.003>